Published in final edited form as:
Ann Biomed Eng. 2012 July ; 40(7): 1419–1433. doi:10.1007/s10439-012-0509-4.

Impact of Residual Stretch and Remodeling on Collagen Engagement in Healthy and Pulmonary Hypertensive Calf Pulmonary Arteries at Physiological Pressures

Lian Tian[1], **Steven R. Lammers**[2], **Philip H. Kao**[1], **Joseph A. Albietz**[2], **Kurt R. Stenmark**[2], **H. Jerry Qi**[1], **Robin Shandas**[1,3], and **Kendall S. Hunter**[3]

[1]Department of Mechanical Engineering, University of Colorado, Boulder, CO, USA

[2]Department of Pediatrics, Division of Critical Care, University of Colorado, Denver, CO, USA

[3]Department of Bioengineering, University of Colorado at Denver, 12700 E. 19th Ave., MS8607, Aurora, CO 80045, USA

Abstract

Understanding the mechanical behavior of proximal pulmonary arteries (PAs) is crucial to evaluating pulmonary vascular function and right ventricular afterload. Early and current efforts focus on these arteries' histological changes, *in vivo* pressure–diameter behavior and mechanical properties under *in vitro* mechanical testing. However, the *in vivo* stretch and stress states remain poorly characterized. To further understand the mechanical behavior of the proximal PAs under physiological conditions, this study computed the residual stretch and the *in vivo* circumferential stretch state in the main pulmonary arteries in both control and hypertensive calves by using *in vitro* and *in vivo* artery geometry data, and modeled the impact of residual stretch and arterial remodeling on the *in vivo* circumferential stretch distribution and collagen engagement in the main pulmonary artery. We found that the *in vivo* circumferential stretch distribution in both groups was nonuniform across the vessel wall with the largest stretch at the outer wall, suggesting that collagen at the outer wall would engage first. It was also found that the circumferential stretch was more uniform in the hypertensive group, partially due to arterial remodeling that occurred during their hypoxic treatment, and that their onset of collagen engagement occurred at a higher pressure. It is concluded that the residual stretch and arterial remodeling have strong impact on the *in vivo* stretch state and the collagen engagement and thus the mechanical behavior of the main pulmonary artery in calves.

Keywords

Residual stretch; Arterial remodeling; Stretch distribution; Collagen engagement

INTRODUCTION

Pulmonary hypertension (PH) is an important cause of morbidity and mortality in children and adults. PH is defined as a chronic, resting mean pulmonary artery pressure (mPAP)

Address correspondence to Kendall S. Hunter, Department of Bioengineering, University of Colorado at Denver, 12700 E. 19th Ave., MS8607, Aurora, CO 80045, USA. ltian22@wisc.edu, Kendall.Hunter@ucdenver.edu.

CONFLICT OF INTEREST

No conflicts of interest, financial or otherwise, are declared by the author(s).

greater than 25 mmHg, yields increases in right ventricular (RV) afterload and is associated with arterial remodeling and eventual RV failure.[9,38,41,56,61] The proximal pulmonary arteries (PAs) in patients with PH display significant vascular remodeling and their mechanical behavior strongly influences pulmonary arterial input impedance, which is a good measure of RV afterload and pulmonary vascular function.[20,21,46,47,61] Moreover, proximal pulmonary vascular stiffness has been shown to correlate very well with the mortality in patients with PH.[10,18,50,52] Therefore, it is important to study the mechanical behavior of the proximal PAs under physiological conditions.[18,38,61]

The chronically hypoxic neonatal calf is a noteworthy and well-established animal model of pediatric PH[56,64] and the mechanics of proximal PAs of this animal model are more representative to that in pediatric PH.[42] Previous studies have shown that under chronic hypoxia conditions the calf proximal PAs underwent wall thickening[56,64] and that the slope of pressure–diameter curve measured in the main pulmonary artery (MPA) increased significantly.[35,64] Such an increase in pressure–diameter slope of calf MPA was found to correlate to the increase of the mechanical properties of MPA.[35] Further, *in vitro* mechanical tests have shown that both the fresh PA tissues and the elastin component of those tissues display increases in their elastic moduli as a result of chronic hypoxia.[41] To accurately evaluate the mechanical behavior of PAs under physiological conditions, however, it is also necessary to determine the *in vivo* stretch or strain (deformation) state. This deformation state is required for accurate prediction of the stress state from an arterial constitutive model and enables the estimation of how arterial components such as elastin, collagen and smooth muscle cells contribute to the artery pressure load-carrying capacity. Moreover, collagen, one of the important passive arterial components, is believed to only carry pressure loading at high stretches; its engagement should result in very stiff arteries, and in turn an increase in RV afterload. Thus, it is useful to determine the stretch state and the collagen engagement of proximal PAs under physiological conditions.

It is well accepted that residual stretch and stress exist in an arterial ring at its no-load state.[6,14,31,34] The residual stretch, though not very large, has a strong influence on the arterial physiological stretch and stress states. The existence of residual stretch can reduce the stretch concentration at the arterial inner wall compared to when residual stretch is not considered, and thus makes the circumferential stretch distribution more uniform.[6,14,31,34] The residual stretch can also increase the inner diameter (ID) at the *in vivo* state and thus decrease the shear stress on the inner wall, which yields a more compliant artery and improves the arterial performance as an elastic reservoir.[48] Accurate estimation of the arterial stretch and stress states at the *in vivo* state is also important to evaluate arterial smooth muscle cell activity.[6] Therefore, it is critical to incorporate the residual stretch or stress when studying the arterial mechanical function.

It is also well known that arterial remodeling can result in geometric, structural and functional changes in the artery. Pulmonary arterial remodeling as a result of chronic hypoxia leads to increases in arterial wall thickness, alterations in the opening angle (OA) or residual stretch, and changes in mechanical properties of the rat proximal PAs.[33] Similarly, the mechanical properties of the mouse proximal PAs were found to be linked to their geometrical and structural changes.[40] The arterial remodeling was believed to restore the *in vivo* circumferential stress to a normal value and to change the arterial stiffness to an optimal level.[28]

To the best of our knowledge, the *in vivo* stretch state and collagen engagement status of calf proximal PAs are still unknown. Considering the importance of residual stretch and arterial remodeling on the mechanical function of the proximal PAs, the goals of this study were (1) to compute the residual stretch in MPAs of neonatal calves and compare the results

between control and hypertensive groups, (2) to model the uniformity of circumferential stretch distribution across vessel wall in MPAs under physiological conditions with residual stretch taken into consideration, and (3) to evaluate the impact of circumferential stretch distribution and arterial remodeling on collagen engagement in MPAs under physiological conditions.

METHODS

In vivo Pressure–Diameter Measurement and Data Processing

All experimental studies were performed after approval by institutional animal care and use committees. Twenty-four newborn Holstein calves weighting between 35 and 50 kg were used with the experiment procedure similar to the previous studies by Stenmark *et al.*[56] and Zuckerman *et al.*[64] Eleven of the calves between 1 and 3 days of the age were put into a large hypobaric chamber at an ambient atmospheric pressure of 430 mmHg (4570 m equivalent air pressure) for 2 weeks to develop PH. The others remained at local ambient pressure (elevation 1500 m; 640 mmHg at Fort Collins, CO) for 2 weeks before testing. Both animal groups underwent hemodynamic and echocardiographic measurements in the chamber at ambient pressure, and were at that pressure for at least an hour before testing to minimize residual hypoxic vasoconstriction. It is noted that although the hypoxic calves were treated under chronic hypoxia, at which mPAP usually exceeded 100 mmHg, we performed the echo measurements at room air condition, i.e., the ambient atmospheric pressure condition. Due to the difficulty in obtaining echo measurement on some calves, both pressure and diameter data were only obtained for five and seven calves, respectively for the control and hypertensive groups. The pulmonary arterial pressures were obtained for eight control and nine hypertensive calves, and the *in vitro* MPA geometry data were obtained for all the calves.

Instantaneous pressure within the middle section of MPA at ambient atmospheric pressure was measured with standard fluid-filled catheters (Transpac IV, Abbott Critical Care Systems, Abbott Park, IL, USA). Ultrasound color Motion-Mode tissue Doppler imaging (CMM-TDI) studies were performed simultaneously using a commercially available scanner (Vivid 5, GE Medical Systems Inc., Waukesha, WI, USA) with a probe appropriate to animal size (2.5 or 3.5 MHz). The ultrasound beam was swept through the long axis of the MPA to find the maximal diameter. A short-axis view was then used to obtain CMM-TDI measurements of instantaneous ID of the MPA, simultaneous with pressure.[35]

The recorded data were post-processed offline using custom-written software (MATLAB, Mathworks Inc., Natick, MA, USA). The program first found the upper and lower wall boundaries in the M-mode image using an image-decimation based method.[36,38] The instantaneous diameter was extracted by integrating velocity data from TDI image along the upper and lower walls. Then the recorded pressure- and extracted diameter-time histories were separated and collected into individual cardiac cycles based on electrocardiographic (ECG) gating. The pressure–diameter data for each cardiac cycle can be obtained from the simultaneous recording of pressure- and diameter-time histories. More detail on the *in vivo* pressure–diameter data acquisition may be found in the previous studies by our group.[10,35,36,38]

The pressure- and diameter-time history data of each cardiac cycle were transferred into frequency domain *via* discrete Fourier transform. Once in frequency domain, the harmonic values of both pressure and diameter up to the fourth mode were averaged on all the cycles and then transferred back to the time domain *via* inverse discrete Fourier transform, with the number of data points in a cycle being the average number of data points of all available cycles. This process yielded an average pressure–diameter loop for each calf. Notably, there

was no significant difference in the average pressure–diameter curve if higher harmonic values of pressure and diameter data were incorporated in the averaging process. The pressure–diameter curve during the increase of pressure (assumed as systole herein) was quite linear; therefore, we only used the systolic portion of the average pressure–diameter curve for analysis, and the smallest and largest pressures in this interval are indicated as the end-diastolic and end-systolic pressures, respectively.

In vitro Artery Geometry Measurement

An MPA ring approximately 5 mm long in the longitudinal direction was obtained from each animal within 1 h of sacrifice. These rings were generally harvested at the straight (longitudinal) section of the pulmonary arterial tube away from curved sections, and then immediately soaked in Calcium and Magnesium-free NaCl-PBS buffer (0.01 mol/L, ionic strength 0.15, pH 7.4) at room temperature. Next, each ring was photographed to obtain a scaled digital image of the cross-sectional area with a Canon camera (EOS Digital Rebel XTi, Canon Inc., Tokyo, Japan) and Canon Macro Lens (Canon Macro Lens EF 100 mm 1:2.8 USM). Each ring was then cut once across the radial direction to obtain the strain- or stress-free state and photographed again on the cross-sectional area after 2 min to allow for possible viscoelastic relaxation. No significant changes were observed in the cross-sectional shape of the sectors (or the opened rings) after the rings had been cut for 2 min.

Ring and sector edge lengths were determined from tracing their images in a custom-written MATLAB image-processing code (MATLAB, Mathworks Inc., Natick, MA). In general, the ring had a clearer edge definition on the inner wall than on the outer wall; thus the inner wall's circumferential length was always traced. For the sector, both the circumferential lengths of inner and outer walls were traced. The thicknesses of the artery at six different circumferential locations of the ring or sector were measured and averaged as the thickness of the ring or sector.

Histology

Biopsies of the cross-sectional calf MPA tissue strips were fixed in 10% buffered formalin, embedded in paraffin wax, and stained with Verhoeff's Van Gieson (VVG). Bright-field photomicrographs of the stained tissues were taken with a SPOT RT-900 digital camera (Diagnostic Instruments Inc., Sterling Heights, MI) mounted on a Nikon TE-200 microscope (Nikon Instruments Inc., Melville, NY; ×4 magnification).

Calculations: Residual Stretch

Figure 1 illustrates the opened sector at strain- or stress-free state with two possible configurations, the closed ring at the no-load state and the deformed ring under physiological conditions. In the figure and in subsequent discussion, cylindrical polar coordinates (r, θ, z) are used to denote a material point in the artery of the no-load or physiological state, and the subscripts or superscripts i and o indicate the inner and outer walls, respectively.

Opening angle is defined as the angle between the two lines connecting the middle point of the inner wall to its tips. Since the configuration of the opened artery in general is not a perfect circular sector shape (indeed, some arteries even turned inside out as shown in Fig. 1b), we did not measure OA directly from the image by finding the middle point of the inner wall and its two tips as in previous studies.[15–17,45] Rather, we assumed a perfect circular sector having the same circumferential lengths of inner and outer walls and thickness as the sector of the real arterial tissue, and calculated OA of the imagined perfect circular sector. Using the geometry of the circular sector,[6,26] the OA of the imagined circular sector can be expressed as

$$\mathrm{OA}=\pi-(L_{\mathrm{o}}-L_{\mathrm{i}})/2H,\quad \text{if } L_{\mathrm{o}}>L_{\mathrm{i}},$$

$$\mathrm{OA}=\pi+(L_{\mathrm{i}}-L_{\mathrm{o}})/2H,\quad \text{if } L_{\mathrm{o}}<L_{\mathrm{i}}, \quad (1)$$

where L_{i}, L_{o} and H are the lengths of inner and outer walls and the thickness of the sector, respectively.

The artery may be considered incompressible.[4,5] As the opened sector deforms to a closed ring at the no-load state (no inner pressure and no axial traction, Fig. 1c) or under physiological conditions (with inner pressure and longitudinal stretch, Fig. 1d), the incompressibility condition of the artery requires[6,26]

$$\lambda_z\pi\left(r^2-r_{\mathrm{i}}^2\right)=(L^2-L_{\mathrm{i}}^2)/4(\pi-OA)\quad \text{if } L_{\mathrm{o}}>L_{\mathrm{i}};$$

$$\lambda_z\pi\left(r^2-r_{\mathrm{i}}^2\right)=(L_{\mathrm{i}}^2-L^2)/4(OA-\pi)\quad \text{if } L_{\mathrm{o}}<L_{\mathrm{i}}, \quad (2)$$

where r is the radius of an arbitrary point in the ring, L is the corresponding circumferential length inside the sector, and λ_z is the longitudinal stretch of the ring.

The circumferential stretch at this arbitrary point of the ring is defined as

$$\lambda_\theta(r)=2\pi r/L \quad (3)$$

Note that Eq. (3) is a general equation to calculate the circumferential stretch. For the ring at the no-load state (Fig. 1c), the ID of the ring is calculated from the measured length of inner wall (l_{i}): ID = $2r_{\mathrm{i}} = l_{\mathrm{i}}/\boldsymbol{\pi}$, and the outer diameter is OD = $2r_{\mathrm{o}} = 2(r_{\mathrm{i}} + h)$, where h is the measured thickness of the ring.

The longitudinal stretches calculated from Eq. (2) using the measured geometry data of the ring and sector were very close to unity for all the arteries. Within measurement error, it is appropriate to assume the longitudinal stretch to be unity for the closed ring at the no-load state.[6,26] In this state the circumferential stretch can then be calculated by Eq. (3) using the geometry data of the artery at its stress-free and no-load states (Figs. 1a or 1b and 1c); this circumferential stretch is called the residual circumferential stretch of the artery at the no-load state.

Applying Eq. (3) to the inner and outer walls, the residual circumferential stretches at the inner and outer walls ($\left(\lambda_\theta^{\mathrm{i}}\right)_{\mathrm{R}}$ and $\left(\lambda_\theta^{\mathrm{o}}\right)_{\mathrm{R}}$, respectively, with subscript R denoting for residual) can be calculated directly from the measured dimensions of the sector and ring:

$$\left(\lambda_\theta^{\mathrm{i}}\right)_{\mathrm{R}}=l_{\mathrm{i}}/L_{\mathrm{i}},\left(\lambda_\theta^{\mathrm{o}}\right)_{\mathrm{R}}=(l_{\mathrm{i}}+2\pi h)/L_{\mathrm{o}}. \quad (4)$$

For the deformed ring under physiological conditions (Fig. 1d), only the ID can be obtained from the *in vivo* pressure–diameter measurement. Using the incompressibility condition of Eq. (2) with measured L_{i} and L_{o} at the stress-free state (Figs. 1a or 1b) and ID ($2r_{\mathrm{i}}$) under physiological conditions (Fig. 1d), the outer diameter ($2r_{\mathrm{o}}$) under physiological conditions

can be calculated for a given longitudinal stretch (λ_z). With all these geometry values at the stress-free and physiological states (Figs. 1a or 1b and 1d), the physiological circumferential stretch of artery can be calculated by Eq. (3). Conversely, if the residual stretches are not considered, the arterial ring at the no-load state (Fig. 1c) is taken as the stress-free or reference state and the physiological circumferential stretch without considering residual stretches could be also estimated using Eqs. (2) and (3) with OA = 0 and L and L_i being the circumferences of the closed arterial ring at the no-load state given in Eq. (2).

In order to characterize the physiological circumferential stretch distribution across the vessel wall, we propose a uniformity index (UI) defined as

$$\mathrm{UI}=\frac{\lambda_\theta^{o}-\lambda_\theta^{i}}{(\lambda_\theta^{o}+\lambda_\theta^{i})/2}, \quad (5)$$

where λ_θ^{i} and λ_θ^{o} are the physiological circumferential stretches at the inner and outer walls, respectively. Note that UI = 0 indicates uniform stretch distribution across the vessel wall.

Calculations: Collagen Model

To investigate whether or not collagen fibers engage under physiological conditions, a simple and reasonable model of the collagen fiber distribution was adopted in this study. Histological studies have shown that collagen fibers in the artery are coiled and wavy at the unloaded state[7,8] and are oriented in different directions.[3,11,12,29,30,53] Nevertheless, these studies have also shown that collagen fibers could display some alignment or mean orientation. Based on these observations many mechanical modeling studies have assumed that the collagen fibers are arranged in helical structures in the arterial tube in the form of two families, within which individual collagen fibers are distributed around mean (i.e., family) orientations.[19,31,51,65] Such a model is based on the constitutive theory for fiber-reinforced composites[54] and well-captures the cylindrically orthotropic mechanical behavior of artery combined with the mechanical behavior of other components of the artery (e.g., elastin). In this study, we adopted this concept assuming the collagen fibers to have two families embedded in the plane perpendicular to the radial direction that are symmetric with respect to the longitudinal axis[31,65]; the angle between the two family fibers at the stress-free state is 2θ as shown in Fig. 2. Although incorporating the dispersion behavior of collagen fibers into a modeling study could provide more accurate prediction of collagen engagement, such model is also very complicated, and is not considered here.

The collagen fiber angle in calf MPA does not exist in the literature. However, our uniaxial mechanical tests (incorporating stretch greater than 1.6) on circumferential and longitudinal MPA strips and equibiaxial tests (stretches greater than 1.25 for both directions) on planar MPA tissues show that at high stretch (i.e., in the collagen-dominant region) the artery is approximately isotropic in these two directions for some MPAs but a little stiffer in the circumferential direction for other MPAs (data from an unpublished study). Moreover, a previous modeling study on calf MPA by our group[39] quantified the parameters for collagen's mechanical behavior and suggested nearly transversely isotropic behavior for MPA. Thus, in this study two collagen fiber angles (θ) of 40° and 45° were adopted in the calculation to examine a relevant range of the collagen engagement stretches under physiological conditions, as explained further below.

Calculations: Collagen Engagement

In uniaxial mechanical test on circumferentially or longitudinally oriented pulmonary arterial strips,[39,41] the typical stress-stretch curve exhibits highly nonlinear behavior with an approximately linear region at low stretch, a transition region and another approximately

linear region at high stretch with higher modulus before fracture.[39,41] The higher modulus in the second linear region is due to the straightening of wavy collagen fibers which then begin to carry load, a process known as collagen engagement. Note that not all the collagen fibers become straightened at the same stretch due to their different waviness at the stress-free state[2,43,44,62,65] as shown in Fig. 2, and this causes a very nonlinear stress-stretch curve in the transition region in which more and more collagen fibers are engaged as the stretch in the arterial wall increases.

A circumferential transition stretch at which the collagen fibers start to carry load can be estimated from uniaxial stress–stretch curves for a circumferential arterial strip.[41] Assuming equal stretches in the radial and longitudinal directions in the uniaxial test below the transition stretch, the stretches in these two directions (Λ) can be calculated from the incompressibility condition, $\Lambda^2\Lambda_\theta^T=1$, where Λ_θ^T is the circumferential transition stretch. Thus, the stretch in the fiber direction at the state of the circumferential transition stretch is

$$\Lambda_{\text{fiber}}^T=\sqrt{(\Lambda_\theta^T)^2\cos^2\theta+\Lambda^2\sin^2\theta}. \quad (6)$$

At the *in vivo* state, the stretch in the fiber direction an arbitrary point of the artery (r) is

$$\lambda_{\text{fiber}}(r)=\sqrt{\lambda_\theta^2(r)\cos^2\theta+\lambda_z^2\sin^2\theta}. \quad (7)$$

When the stretch of fiber calculated with Eq. (7) is larger than the engaged stretch of fiber, Λ_{fiber}^T, collagen at those locations will engage. Given a longitudinal stretch, the critical engagement stretch in the circumferential direction can be obtained from Eqs. (6) and (7) as $\lambda_\theta^T=\sqrt{(\Lambda_\theta^T)^2+\Lambda^2\tan^2\theta-\lambda_z^2\tan^2\theta}$.

In a previous study by our group,[41] the circumferential transition stretches (Λ_θ^T) were estimated from the uniaxial test on the PAs as 1.49 ± 0.08 and 1.51 ± 0.10 for control and hypertensive groups, respectively and there was no significant difference in Λ_θ^T between the two groups; thus a circumferential transition stretch of 1.5 was used in Eq. (6) for the collagen engagement calculation for all the arteries collected from both groups under physiological conditions.

The *in vivo* MPA longitudinal stretch was not measured. Therefore, several longitudinal stretches varying from 1.0 to 1.5 were taken for the calculations in this study. However, previous studies showed that the measured mean *in vivo* longitudinal stretches were 1.15 for proximal mouse aorta[23] and 1.2 for the descending region of the canine and porcine aortas.[25] Therefore, the *in vivo* longitudinal stretch of the calf MPA is believed to be small. The representative value of 1.1 was chosen whenever a specific *in vivo* MPA longitudinal stretch was relevant for results presentation.

Statistics

All the data are presented as mean ± SD unless specified otherwise. The two-tailed two-sample *t*-test assuming normality in the data with variances determined from an *F*-test was used to compare the geometric dimensions, MPA residual stretches, the uniformity indices (UIs), and the physiological circumferential stretches between control and hypertensive groups. Equivalence tests[27] were performed to compare the MPA geometric dimensions and residual stretches between control and hypertensive groups assuming the equivalence

interval equal to 10% of the average value of the control group. A mixed-effects regression method was used to model the UI and *in vivo* outer-walled circumferential stretch at end diastole and end systole as a function of pressure. The confidence level was set at95% for all tests. The regression analyses were performed with SAS software (SAS Institute, Cary, NC), while all the other statistical analyses were performed with MATLAB software (MATLAB, Mathworks Inc., Natick, MA).

RESULTS

Comparisons of the mPAP, morphology, OA and residual circumferential stretches at the inner and outer walls of MPA between control and hypertensive groups are presented in Table 1. Note that we obtained geometry data for all twenty-four calves, but only obtained PAP from eight control and nine hypertensive calves. mPAP increases significantly from the control to hypertensive group. There is no significant difference in the MPA ID at the no-load state between control and hypertensive groups and the IDs of the two groups are statistically equivalent. Both the arterial wall thickness and the thickness to ID ratio have significant increases from control to hypertensive group. The differences in OA and the residual circumferential stretches at the inner and outer walls between the two groups are not significant, and the residual stretches at the inner and outer walls are statistically equivalent between the two groups.

Arterial Residual Stretch and Morphometry

A representative residual circumferential stretch distribution across the MPA wall is shown in Fig. 3. At the no-load state, the artery is under compression at the inner wall and under tension at the outer wall, and the stretch distribution is found to be approximately linear. Therefore, knowing the residual circumferential stretches at the inner and outer wall is enough to obtain an approximate linear residual circumferential stretch distribution. Figure 4 displays representative circumferential stretch distributions of the MPA at end-diastolic and end-systolic pressures. The distributions are shown for a single *in vivo* longitudinal stretch of 1.1 and both with and without consideration of residual circumferential stretch. Figures 4a and 4b show these representative distributions from the control (Fig. 4a) and hypertensive (Fig. 4b) groups, respectively. When the residual circumferential stretch is not incorporated (i.e., the closed ring is taken as the stress-free state and is noted as ‘close ring’ in the figure legends), the circumferential stretch distribution is not uniform and the stretch is largest at the inner wall at both pressures for both calves. However, when the residual circumferential stretch is incorporated (i.e., the open sector is taken as the stress-free state, and is noted as ‘open ring’ in the figure legends), the largest circumferential stretch is seen at the outer wall at both pressures for both calves.

Note that the physiological circumferential stretch of a control calf MPA at end diastole with residual stretch incorporated (the curve corresponding to the open ring at end diastole in Fig. 4a) is similar to the residual stretch in Fig. 3. This is not surprising because at the physiological state the longitudinal stretch (1.1) tends to decrease the diameter while the inner pressure tends to increase the diameter compared to the no-load state (longitudinal stretch of 1.0 with zero inner pressure); thus the diameter at a low end-diastolic pressure does not change substantially compared to that of the no-load state.

Uniformity Index

To examine the degree of uniformity in the physiological circumferential stretch distribution, the uniformity indices (UIs) at the end-diastolic and end-systolic pressures for control and hypertensive groups are shown in Fig. 5. These UIs are plotted for longitudinal stretches varying from 1 to 1.5, and all incorporate the effects of residual circumferential

stretch. The UI standard deviations at each longitudinal stretch and for each group are not shown in the figure, and decrease slightly as the longitudinal stretch increases. The ranges of the standard deviations at these six longitudinal stretches are 0.093–0.104 (mean: 0.098 ± 0.004) and 0.088–0.097 (mean: 0.092 ± 0.004) for the control group at end diastole and end systole respectively, and 0.042–0.046 (mean: 0.042 ± 0.003) and 0.039–0.042 (mean: 0.039 ± 0.002) for hypertensive group at end diastole and end systole respectively.

As seen from Fig. 5, if the longitudinal stretch is larger, the mean UIs become smaller at both pressures for both groups. It is also found that the circumferential stretch is always greatest at the outer wall for all the calves in their physiological pressure range. The mean UIs of the hypertensive group are about 50% smaller than those of the control group at both pressures for these six longitudinal stretches from 1 to 1.5 ($P = 0.052–0.056$ and $P = 0.092–0.099$ at end diastole and end systole, respectively). Note that one control calf had abnormally high pressure (an outlier indicated by Grubbs' test on 8 control calves, $P < 0.05$); if this calf is excluded, significant differences were seen between the two groups at all six longitudinal stretches ($P < 0.033$).

Figure 6 shows the mixed-effects regression between UI and the MPA blood pressure at the *in vivo* longitudinal stretch of 1.1. The two endpoints of each segment represent the calf MPA UIs at end diastole and end systole, respectively. UI decreases as the pressure increases for both groups but with greater decreasing trend in the control group. The difference in the decreasing trend between the two groups predicted from the mixed-effects model is statistically significant ($P = 0.0069$). The extrapolations of the two regression lines from the model indicate that the UI will be zero around 80 mmHg for control group and larger than 120 mmHg for hypertensive group.

In vivo Circumferential Stretch and Collagen Engagement

The mean circumferential stretches at the inner and outer walls of the artery at different longitudinal stretches at end-diastolic and end-systolic pressures for both groups are shown in Figs. 7a and 7b, respectively. The standard deviations of the circumferential stretches at each longitudinal stretch and for each group are not shown in the figure, and increase slightly as the longitudinal stretch increases. The ranges of the standard deviations at these six longitudinal stretches are 0.098–0.102 (mean: 0.100 ± 0.002) and 0.113–0.119 (mean: 0.116 ± 0.002) for control group at the outer wall at end diastole and end systole respectively, and 0.096–0.103 (mean: 0.100 ± 0.002) and 0.101–0.106 (mean: 0.103 ± 0.002) for hypertensive group at the outer wall at end diastole and end systole respectively. Note that the inner wall stretch is constant across the *in vivo* longitudinal stretches because it is defined by our *in vivo* measurements; thus the standard deviations of the inner wall circumferential stretches at these six longitudinal stretches are identical and are given by 0.142 and 0.165 for the control group at end diastole and end systole respectively, and 0.122 and 0.126 for the hypertensive group at end diastole and end systole respectively. The critical circumferential stretches for collagen to engage with collagen fiber angles at 40° and 45° are also shown in the figures as dashed and dotted curves respectively. Note that the critical circumferential stretch decreases nonlinearly as the longitudinal stretch or collagen fiber angle increases, which can be expected from the equation for the critical circumferential stretch.

As a consequence of the disease state which increases the pressure loading of the vessels, the mean circumferential stretches at the inner and outer walls of the hypertensive group arteries are greater than those of the control group at both pressures (Fig. 7; $P = 0.026$ and $P = 0.055$ for inner wall stretch at end diastole and end systole, respectively; $P = 0.045–0.052$ and $P = 0.09–0.10$ for outer wall stretch at end diastole and end systole, respectively). Note that one control calf had abnormally high pressure (an outlier as mentioned previously); if

this calf is excluded, significant significances were seen between the two groups at all six longitudinal stretches ($P < 0.019$). As longitudinal stretch increases, the critical engagement stretches decrease at both collagen fiber angles (40° and 45°). The mean circumferential stretches at the outer wall also decrease, but to a smaller degree. For the control group MPAs at both end-diastolic and endsystolic pressures, the circumferential stretch is smaller than the critical engagement stretch at small longitudinal stretch and around the critical engagement stretch at larger longitudinal stretch, depending on the fiber angle. For the hypertensive group MPAs at the end-diastolic pressure, the circumferential stretch at the outer wall is around the critical engagement stretch at small longitudinal stretch, while at larger longitudinal stretch the circumferential stretch across the whole artery can be larger than the critical engagement stretch. Similarly, at end-systolic pressure, the circumferential stretch across the whole artery is around or larger than the critical engagement stretch at all longitudinal stretch values.

Figure 8 shows the *in vivo* circumferential stretch modeled as a function of the MPA blood pressure at an *in vivo* longitudinal stretch of 1.1. The two endpoints of each segment represent the *in vivo* circumferential stretches at the outer wall of a calf MPA at the end diastole and end systole, respectively. The mixed-effects model predicts that under physiological conditions collagen in MPA starts to engage around 45 mmHg for the control group and around 60 mmHg for the hypertensive group. The slopes of these models are statistically different ($P = 0.0026$).

Histology

Representative histological images of control and hypertensive MPA tissues are shown in Fig. 9. The adventitial layer is deposited with a large amount of collagen fibers and has similar thickness fraction for both calves; additionally there are much more collagen fibers deposited in the adventitial layer than in the medial and intimal layers for both calves. Moreover, a previous study by our group[60] has shown that the thickness fraction of the adventitial layer is 0.31 ± 0.06 for 6 control calves and 0.30 ± 0.03 for 5 hypertensive calves. No significant change in the thickness fraction was found, although the arterial wall thickness increased in the hypertensive group as noted previously in Table 1.

DISCUSSION

The residual stretch of the conduit arteries has been found to be important in accurately estimating the arterial *in vivo* strain state,[6,31] in reducing the *in vivo* strain gradient across the vessel wall,[6,14,31,34] and in making arteries more compliant thereby improving their performance as elastic reservoirs.[48] Arterial remodeling, including the changes of geometry, structure and properties in response to hypertension, has also been suggested to restore the arterial wall stress to a normal value and to change the arterial stiffness to an optimal level based on several studies on rat aortic and carotid arteries, human carotid and radial arteries, and veins in rat, rabbit and swine.[28] However, there are still no studies on the impact of the residual stretch and arterial remodeling in large mammal PAs, which are more complex than that of rodent species and potentially more relevant to human disease.[55] Thus, the purpose of this study was to investigate the impact of arterial remodeling due to chronic hypoxia on the residual stretch, the circumferential stretch distribution and collagen engagement in calf MPAs under physiological pressure conditions. To the best of our knowledge, this paper provides the first such study of these parameters in the MPAs of normal and hypertensive calves. Several interesting and important results are discussed in detail as follows.

Morphometry and Residual Stretch

Similar to rodent proximal PAs in previous studies,[33,40,60] the arterial wall thickness of calf MPA was found to increase significantly due to chronic hypoxia, which is also consistent to the previous studies on calf MPAs.[41,64] The OAs of calf MPAs did not change significantly in response to chronic hypoxia and have an average of 128° ± 31° for the pooled control and hypertensive calves. Similarly, the residual stretches at the inner and outer wall did not change significantly. In the rat MPA, however, significant changes due to chronic hypoxia were also seen in OAs, which were larger than 180°[16,33] in MPA for both control and hypertensive groups; the residual stretches in rat MPA are expected to change significantly from control to hypertensive group because of the dramatic change of OA. Such differences between rat and calf MPAs may be due to their different arterial remodeling mechanisms[55] or their different developmental stages as rats and calves were adult and neonatal respectively during the test.[57]

Circumferential Stretch Distribution and Uniformity

Under physiological conditions with residual stretches considered, the stress concentration at the inner wall seen in Fig. 4 disappeared (as expected) and the circumferential stretch increased approximately linear from inner to outer wall. Neglecting to include the residual stretch completely reverses the stretch trend such that maximum stretch occurs at the inner wall (Fig. 4), and such stretch distribution makes the artery mechanically stiffer.[48] Thus, the existence of residual stretch yields a more compliant artery, and proper consideration of the residual stretch when modeling the system is vital for proper attribution of the roles of elastin and collagen to the load-carrying capabilities of the vessel.

The circumferential stretch distribution was not uniform within the physiological pressure range for both groups, but the hypertensive group had a more uniform circumferential stretch distribution, presumably due to arterial remodeling and higher physiological pressures (Fig. 5). OAs for both groups were less than 180°, which satisfies the theoretical requirement for uniform circumferential stretch.[24] However, uniformity did not occur for either group in their respective physiological pressure ranges. This is in agreement with some other studies; for example, the nonuniformity of the circumferential stretch was also found in pig coronary arteries and the aorta and its branches, all with OAs less than 180°.[24] Therefore, the uniform circumferential stretch hypothesis[59] may be invalid for some arteries and should be employed with caution, because the accuracy of the arterial strain state can be important when the strain or stress distribution across the vessel is used to estimate smooth muscle activity, which depends on its local strain and stress states.[13]

At a longitudinal stretch of 1.1, the uniformity indices (UIs) of the hypertensive group are about 50% less than the control group indices within each group's physiological pressure range (Fig. 5). All UIs are about 0.1 or greater, which indicates that the circumferential stretch at the outer wall is at least 10% larger than at the inner wall as can be seen from Eq. (5). As pressure increases, the circumferential stretch across vessel wall becomes more uniform for each group but with a greater trend in the control group (Fig. 6). The change of UI in the hypertensive group is less than that in the control group, again presumably due to arterial remodeling. Without such changes, the *in vivo* circumferential stretch of the MPAs in the hypertensive group, predicted from the trend in the control group, would be greatest at the inner wall in their physiological pressure range (i.e., <80 mmHg; Fig. 6a). Such stretch distribution would result in higher MPA stiffness and thus higher RV afterload. Therefore, arterial remodeling in the hypertensive calves restores the stretch distribution with largest stretch at the outer wall and tries to restore the arterial compliance.

Collagen Engagement and Histology

As seen from Fig. 7, knowing only the circumferential transition stretch (Λ_θ^T) estimated from the uniaxial test is not enough to determine collagen engagement under physiological conditions; also required are the *in vivo* longitudinal stretch and the modeled collagen fiber angle. Nevertheless, the collagen engagement is relatively insensitive to the longitudinal stretch within a reasonable, physiologically relevant range (1.1–1.3) (Fig. 7). Therefore, we performed further calculation and analysis at only a single chosen longitudinal stretch of 1.1, with the expectation that other values should provide us with similar results and conclusions. At a longitudinal stretch of 1.1 and a collagen fiber angle of 45°, the control calves do not display significant collagen engagement even at the end-systolic pressure (Fig. 8a), while most of the hypertensive calves begin to engage collagen at the end-diastolic pressure and are fully engaged at the end-systolic pressure (Fig. 8b). This observation is consistent to a previous study by our group[41] that used Lame's equation to estimate the *in vivo* circumferential strain and found that the circumferential strains for the hypertensive calves at the end diastole are close to the transition strain indicating collagen engagement at end diastole. This observation is also supported by our previous study[35] which shows that the slopes of *in vivo* pressure–diameter curves and elastic moduli for hypertensive calves are much larger than those of control calves indicating that collagen is potentially engaged in the hypertensive calves at least at end systole but not at any physiological pressures in the control calves. Addressing the uncertainty in the fiber angle, we note that if it were small (<35°), no collagen engagement for hypertensive calves would occur even at end systole, while a large angle (>55°) leads to collagen engagement even for control calves. Neither case is supported by our previous studies.[35,39,41] Therefore, the range of collagen fiber angles explored herein (40°–45°) seems reasonable.

Because of the approximately linear increase of the circumferential stretch from the inner to outer wall of artery, the collagen near the outer wall—e.g., in the adventitial layer—will engage earlier than that nearer to the inner wall and the media layer. As a result of the collagen engagement, the MPAs in hypertensive calves are expected to operate at the stiffer state which is consistent to the previous study that found the higher pressure–diameter modulus in hypertensive calves than in control calves.[35] This also implies that the smaller slope of UI against pressure seen in the hypertensive group (Fig. 6) could be partially due to reduced MPA distensibility because of collagen engagement. Moreover, reduced or negligible collagen engagement in control calves indicates that elastin is the mechanically dominant arterial component in the physiological pressure region. Conversely, collagen engagement in the hypertensive calves implies that both elastin and collagen play a role in carrying the pressure load and contribute to RV afterload, and it is possible that collagen is the primary load-carrying extracellular matrix (ECM) at high pressures. These findings confirm previous speculation regarding the contribution of individual ECM components (primarily elastin and collagen) to the mechanical function of calf proximal PAs under physiological conditions.[41]

Regressing change in circumferential stretch of the outer wall as a function of pressure, as shown in Fig. 8, predicted that collagen starts to engage at higher pressures in the hypertensive group than that in the control group; recall that a previous study[41] demonstrated that the critical engagement stretches under uniaxial test are the same for both groups. Remodeling is known to reduce stretch in the hypertensive group compared to the control group at a given stress in the uniaxial testing, and it was also speculated that remodeling also results in the decrease of the arterial diameter and thus the stretch at the same physiological pressure[41]; such speculation is confirmed in this study. Remodeling delays the collagen engagement to higher pressure levels, suggesting that it is a compensatory mechanism that yields a less stiff artery compared to what would be obtained

in the unchanged, control arteries at the physiological hypertensive pressure range: fully engaged collagen. This suggests that the arterial remodeling tries to maintain Windkessel function—or the arterial elastic reservoir—and to reduce RV afterload. However, the remodeling is limited in that severely hypertensive calves can still undergo significant collagen engagement.

Histological sections of both control and hypertensive calf arteries (Fig. 9) show that the majority of collagen present in the vessels lies near the outer wall. Although arterial wall thickness increased as a result of chronic-hypoxia induced arterial remodeling, no significant changes in the radial distribution of collagen were seen. Such a constant collagen distribution across the thickness of the MPA may be linked to the stretch distribution across the vessel wall and is explained as follows. For the control calves with relatively low physiological pressure, little to no collagen engages and elastin is the dominant component for carrying load, yielding a very compliant artery. For the control calves during exercise or the hypertensive calves at their physiological (hypertensive) pressure, collagen in the adventitial layer engages first due to the largest stretch at the outer wall, which in turn is due to the residual stretch and arterial remodeling. While the residual stretch makes the artery more compliant[48] and arterial remodeling tries to restore the compliant arterial behavior for hypertensive calves, such a collagen distribution and its resulting engagement characteristics can effectively protect the artery from over dilation at high pressure.[1]

The implications of collagen engagement on the diagnosis and treatment of PH are still being explored. Given that collagen engagement is associated with increased afterload through increasing pulse pressure (and the higher harmonics of impedance), a patient who maintains functional elastin, through either adaptation (as is seen in the neonatal calf) or simply due to lower pressures, should have a better disease outcome compared to an individual who engages collagen. Indeed, one sees poorer outcomes in scleroderma/systemic sclerosis (SSc) associated PAH, even compared to IPAH patients with similar PVR; emergent data suggests SSc-PAH is associated with significant vascular stiffening and increases in the higher harmonics of impedance. Our group has developed a means to detect vascular stiffening using a minimally invasive approach[35] has begun to show that stiffness alone is prognostic[37] in addition to examining whether such a measurement modality is sufficiently sensitive to detect collagen engagement.

Limitations

Several limitations are noted in our study. First, the MPA outer diameter, thickness, and longitudinal stretch were not measured in the intact animal or *in situ* due to technical difficulties. The knowledge of these MPA geometric parameters *in situ* will facilitate the accurate determination of the *in vivo* circumferential stretch. Secondly, a simple collagen model assuming two-family fibers was used. Since the collagen distribution in the artery is dispersed in both fiber orientation and location,[19] a more advanced and sophisticated collagen model considering such fiber distribution may provide more accurate estimation of collagen engagement under physiological conditions. Finally, the artery was assumed homogeneous for the estimation of the residual stretch distribution. Earlier studies have shown that one-layer homogeneous material models of artery mechanics can still provide reasonably accurate stretch estimation.[26] However, the artery has three layers with different histology and several components with different properties,[19,31,34,49] and the opened sector might not be considered as a strain- or stress-state.[22,32,58,63] All these limitations remain to be considered in future studies.

Conclusion

We have computed the residual circumferential stretch in calf MPA and modeled the impacts of the residual circumferential stretch and arterial remodeling on the circumferential stretch distribution and collagen engagement of calf MPAs under physiological conditions for control and hypertensive groups. In the calf model of PH, remodeling in the MPA increases the elastin modulus at low stretches,[41] which we have shown in turn (1) maintains high compliance of the artery *in vivo* by preventing collagen engagement at the new higher operating pressures and (2) changes the rate at which the UI approaches zero, thereby retaining the appropriate, protective strain distribution imparted by the residual stretch. In conclusion, residual stretch and arterial remodeling have a strong impact on the mechanical behavior of the calf MPA under physiological conditions, and understanding those impacts is important to evaluate PA hemodynamics and RV afterload.

Acknowledgments

This study was supported in part by grants from the National Institutes of Health (T32-HL072738, K24-HL081506, K25-HL094749, and SCCOR-HL084923).

REFERENCES

1. Burton AC. Relation of structure to function of the tissues of the wall of blood vessels. Physiol. Rev. 1954; 34:619–642. [PubMed: 13215088]
2. Cacho F, Elbischger PJ, Rodríguez JF, Doblaré M, Holzapfel GA. A constitutive model for fibrous tissues considering collagen fiber crimp. Int. J. Nonlinear Mech. 2007; 42:391–402.
3. Canham PB, Finlay HM, Dixon JG, Boughner DR, Chen A. Measurements from light and polarised light microscopy of human coronary arteries fixed at distending pressure. Cardiovasc. Res. 1989; 23:973–982. [PubMed: 2611805]
4. Carew TE, Vaishnav RN, Patel DJ. Compressibility of the arterial wall. Circ. Res. 1968; 23:61–68. [PubMed: 5661939]
5. Chuong CJ, Fung YC. Compressibility and constitutive equation of arterial wall in radial compression experiments. J. Biomech. 1984; 17:35–40. [PubMed: 6715386]
6. Chuong CJ, Fung YC. On residual stresses in arteries. J. Biomech. Eng. 1986; 108:189–192. [PubMed: 3079517]
7. Clark JM, Glagov S. Transmural organization of the arterial media. The lamellar unit revisited. Arterioscler. Thromb. Vasc. Biol. 1985; 5:19–34.
8. Dingemans KP, Teeling P, Lagendijk JH, Becker AE. Extracellular matrix of the human aortic media: an ultrastructural histochemical and immunohistochemical study of the adult aortic media. Anat. Rec. 2000; 258:1–14. [PubMed: 10603443]
9. Durmowicz AG, Stenmark KR. Mechanisms of structural remodeling in chronic pulmonary hypertension. Pediatr. Rev. 1999; 20:91–102.
10. Dyer KL, Lanning CJ, Das BB, Ivy DD, Shandas R. Development and validation of a non-invasive color M-mode tissue Doppler imaging technique for measuring pulmonary artery compliance: in vitro and clinical studies. J. Am. Soc. Echocardiogr. 2006; 19:403–412. [PubMed: 16581479]
11. Elbischger PH, Bischof H, Regitnig P, Holzapfel GA. Automatic analysis of collagen fiber orientation in the outermost layer of human arteries. Pattern Anal. Appl. 2004; 7:269–284.
12. Finlay HM, McCullough L, Canham PB. Three-dimensional collagen organization of human brain arteries at different transmural pressures. J. Vasc. Res. 1995; 32:301–312. [PubMed: 7578798]
13. Fung, YC. Biodynamics: Circulation. New York: Springer; 1984.
14. Fung YC. What are the residual stresses doing in our blood vessels? Ann. Biomed. Eng. 1991; 19:237–249. [PubMed: 1928868]
15. Fung YC, Liu SQ. Change of residual strains in arteries due to hypertrophy caused by aortic constriction. Circ. Res. 1989; 65:1340–1349. [PubMed: 2805247]

16. Fung YC, Liu SQ. Changes of zero-stress state of rat pulmonary arteries in hypoxic hypertension. J. Appl. Physiol. 1991; 70:2455–2470. [PubMed: 1885439]
17. Fung YC, Liu SQ. Strain distribution in small blood vessels with zero-stress state taken into consideration. Am. J. Physiol. Heart Circ. Physiol. 1992; 262:H544–H552.
18. Gan CTJ, Lankhaar JW, Westerhof N, Marcus JT, Becker A, Twisk JWR, Boonstra A, Postmus PE, Vonk-Noordegraaf A. Noninvasively assessed pulmonary artery stiffness predicts mortality in pulmonary arterial hypertension. Chest. 2007; 132:1906–1912. [PubMed: 17989161]
19. Gasser TC, Ogden RW, Holzapfel GA. Hyperelastic modelling of arterial layers with distributed collagen fibre orientations. J. R. Soc. Interface. 2006; 3:15–35. [PubMed: 16849214]
20. Grant BJB, Lieber BB. Clinical significance of pulmonary arterial input impedance. Eur. Respir. J. 1996; 9:2196–2199. [PubMed: 8947059]
21. Grant BJB, Paradowski LJ, Fitzpatrick JM. Effect of perivascular electromagnetic flow probes on pulmonary hemodynamics. J. Appl. Physiol. 1988; 65:1885–1890. [PubMed: 3053589]
22. Greenwald SE, Moore JE, Rachev A, Kane TPC, Meister JJ. Experimental investigation of the distribution of residual strains in the artery wall. J. Biomech. Eng. 1997; 119:438–444. [PubMed: 9407283]
23. Guo X, Kono Y, Mattrey R, Kassab GS. Morphometry and strain distribution of the C57BL/6 mouse aorta. Am. J. Physiol. Heart Circ. Physiol. 2002; 283:H1829–H1837. [PubMed: 12384460]
24. Guo X, Lu X, Kassab GS. Transmural strain distribution in the blood vessel wall. Am. J. Physiol. Heart Circ. Physiol. 2005; 288:H881–H886. [PubMed: 15650158]
25. Han HC, Fung YC. Longitudinal strain of canine and porcine aortas. J. Biomech. 1995; 28:637–641. [PubMed: 7775500]
26. Han HC, Fung YC. Direct measurement of transverse residual strains in aorta. Am. J. Physiol. Heart Circ. Physiol. 1996; 39:H750–H759.
27. Hatch JP. Using statistical equivalence testing in clinical biofeedback research. Biofeedback Self-Regul. 1996; 21:105–119. [PubMed: 8805961]
28. Hayashi K, Naiki T. Adaptation and remodeling of vascular wall; biomechanical response to hypertension. J. Mech. Behav. Biomed. Mater. 2009; 2:3–19. [PubMed: 19627803]
29. Holzapfel GA. Determination of material models for arterial walls from uniaxial extension tests and histological structure. J. Theor. Biol. 2006; 238:290–302. [PubMed: 16043190]
30. Holzapfel, GA. Collagen in arterial walls: biomechanical aspects. In: Heidelberg, FP., editor. Collagen. Structure and Mechanics. Vol. Chapter 11. Berlin: Springer; 2008. p. 285-324.
31. Holzapfel GA, Gasser TC, Ogden RW. A new constitutive framework for arterial wall mechanics and a comparative study of material models. J. Elasticity. 2000; 61:1–48.
32. Holzapfel GA, Sommer G, Auer M, Regitnig P, Ogden RW. Layer-specific 3D residual deformations of human aortas with non-atherosclerotic intimal thickening. Ann. Biomed. Eng. 2007; 35:530–545. [PubMed: 17285364]
33. Huang W, Sher YP, Delgado-West D, Wu JT, Peck K, Fung YC. Tissue remodeling of rat pulmonary artery in hypoxic breathing. I. Changes of morphology, zero-stress state, and gene expression. Ann. Biomed. Eng. 2001; 29:535–551. [PubMed: 11501619]
34. Humphrey, JD. Cardiovascular Solid Mechanics. Cells, Tissues, and Organs. New York: Springer; 2002.
35. Hunter KS, Albietz JA, Lee PF, Lanning CJ, Lammers SR, Hofmeister SH, Kao PH, Qi HJ, Stenmark KR, Shandas R. In vivo measurement of proximal pulmonary artery elastic modulus in the neonatal calf model of pulmonary hypertension: development and ex vivo validation. J. Appl. Physiol. 2010; 108:968–975. [PubMed: 20093662]
36. Hunter KS, Gross JK, Lanning CJ, Kirby KS, Dyer KL, Ivy DD, Shandas R. Noninvasive methods for determining pulmonary vascular function in children with pulmonary arterial hypertension: application of a mechanical oscillator model. Congenit. Heart Dis. 2008; 3:106–116. [PubMed: 18380759]
37. Hunter KS, Lanning CJ, Kirby KS, Ivy DD, Shandas R. In Vivo pulmonary vascular stiffness obtained from color M-Mode tissue Doppler imaging and pressure measurements predicts clinical outcomes better than indexed pulmonary vascular resistance in pediatric patients with pulmonary arterial hypertension. Circulation. 2008; 118:S879–S879.

38. Hunter KS, Lee PF, Lanning CJ, Ivy DD, Kirby KS, Claussen LR, Chan KC, Shandas R. Pulmonary vascular input impedance is a combined measure of pulmonary vascular resistance and stiffness and predicts clinical outcomes better than pulmonary vascular resistance alone in pediatric patients with pulmonary hypertension. Am. Heart J. 2008; 155:166–174. [PubMed: 18082509]
39. Kao PH, Lammers SR, Tian L, Hunter K, Stenmark KR, Shandas R, Qi HJ. A microstructurally driven model for pulmonary artery tissue. J. Biomech. Eng. 2011; 133 051002.
40. Kobs RW, Muvarak NE, Eickhoff JC, Chesler NC. Linked mechanical and biological aspects of remodeling in mouse pulmonary arteries with hypoxia-induced hypertension. Am. J. Physiol. Heart Circ. Physiol. 2005; 288:H1209–H1217. [PubMed: 15528223]
41. Lammers SR, Kao PH, Qi HJ, Hunter K, Lanning C, Albietz J, Hofmeister S, Mecham R, Stenmark KR, Shandas R. Changes in the structure-function relationship of elastin and its impacts on the proximal pulmonary arterial mechanics of hypertensive calves. Am. J. Physiol. Heart Circ. Physiol. 2008; 295:H1451–H1459. [PubMed: 18660454]
42. Lammers, SR.; Kao, P.; Tian, L.; Hunter, K.; VanRheen, Z.; Albietz, J.; Lanning, C.; Hoffmeister, S.; Miyamoto, s; Kulik, T.; Qi, HJ.; Shandas, R.; Stenmark, K. Conduit arteries in small and large mammals express different material property changes in response to hypoxia-induced pulmonary hypertension. ATS International Conference; May 14–19; New Orleans, LA. 2010.
43. Lanir Y. A structural theory for the homogeneous biaxial stress-strain relationships in flat collagenous tissues. J. Biomech. 1979; 12:423–436. [PubMed: 457696]
44. Lanir Y. Constitutive equations for fibrous connective tissues. J. Biomech. 1983; 16:1–12. [PubMed: 6833305]
45. Liu SQ, Fung YC. Zero-stress states of arteries. J. Biomech. Eng. 1988; 110:82–84. [PubMed: 3347028]
46. Milnor WR. Arterial impedance as ventricular afterload. Circ. Res. 1975; 36:565–570. [PubMed: 1122568]
47. Milnor WR, Conti CR, Lewis KB, O'Rourke MF. Pulmonary arterial pulse wave velocity and impedance in man. Circ. Res. 1969; 25:637–649. [PubMed: 5364641]
48. Rachev A, Greenwald SE. Residual strains in conduit arteries. J. Biomech. 2003; 36:661–670. [PubMed: 12694996]
49. Roach MR, Burton AC. The reason for the shape of the distensibility curves of arteries. Can. J. Biochem. Physiol. 1957; 35:681–690. [PubMed: 13460788]
50. Rodés-Cabau J, Domingo E, Román A, Majó J, Lara B, Padilla F, Anívarro I, Angel J, Tardif JC, Soler-Soler J. Intravascular ultrasound of the elastic pulmonary arteries: a new approach for the evaluation of primary pulmonary hypertension. Heart. 2003; 89:311–315. [PubMed: 12591838]
51. Rodríguez JF, Ruiz C, Doblaré M, Holzapfel GA. Mechanical stresses in abdominal aortic aneurysms: influence of diameter, asymmetry, and material anisotropy. J. Biomech. Eng. 2008; 130 021023.
52. Sanz J, Kariisa M, Dellegrottaglie S, Prat-Gonzalez S, Garcia MJ, Fuster V, Rajagopalan S. Evaluation of pulmonary artery stiffness in pulmonary hypertension with cardiac magnetic resonance. JACC Cardiovasc. Imaging. 2009; 2:286–295. [PubMed: 19356573]
53. Schmid F, Sommer G, Rappolt M, Schulze-Bauer CAJ, Regitnig P, Holzapfel GA, Laggner P, Amenitsch H. In situ tensile testing of human aortas by time-resolved small-angle X-ray scattering. J. Synchrotron Radiat. 2005; 12:727–733. [PubMed: 16239740]
54. Spencer, AJM. Constitutive theory for strongly anisotropic solids. In: Spencer, AJM., editor. Continuum Theory of the Mechanics of Fiber-Reinforced Composites. Vol. Chapter 2. Wien, New York: Springer; 1984. p. 23-82.CISM Course and Lectures No. 282, International Centre for Mechanical Sciences
55. Stenmark KR, Fagan KA, Frid MG. Hypoxiainduced pulmonary vascular remodeling—cellular and molecular mechanisms. Circ. Res. 2006; 99:675–691. [PubMed: 17008597]
56. Stenmark KR, Fasules J, Hyde DM, Voelkel NF, Henson J, Tucker A, Wilson H, Reeves JT. Severe pulmonary hypertension and arterial adventitial changes in newborn calves at 4300 m. J. Appl. Physiol. 1987; 62:821–830. [PubMed: 3558241]

57. Stenmark KR, Mecham RP. Cellular and molecular mechanisms of pulmonary vascular remodeling. Annu. Rev. Physiol. 1997; 59:89–144. [PubMed: 9074758]
58. Stergiopulos N, Vulliemoz S, Rachev A, Meister JJ, Greenwald SE. Assessing the homogeneity of the elastic properties and composition of the pig aortic media. J. Vasc. Res. 2001; 38:237–246. [PubMed: 11399896]
59. Takamizawa K, Hayashi K. Strain energy density function and uniform strain hypothesis for arterial mechanics. J. Biomech. 1987; 20:7–17. [PubMed: 3558431]
60. Tian L, Lammers SR, Kao PH, Reusser M, Stenmark KR, Hunter KS, Qi HJ, Shandas R. Linked opening angle and histological and mechanical aspects of the proximal pulmonary arteries of healthy and pulmonary hypertensive rats and calves. Am. J. Physiol. Heart Circ. Physiol. 2011; 301:H1810–H1818. [PubMed: 21856906]
61. Weinberg CE, Hertzberg JR, Ivy DD, Kirby KS, Chan KC, Valdes-Cruz L, Shandas R. Extraction of pulmonary vascular compliance, pulmonary vascular resistance, and right ventricular work from single-pressure and Doppler flow measurements in children with pulmonary hypertension: a new method for evaluating reactivity—in vitro and clinical studies. Circulation. 2004; 110:2609–2617. [PubMed: 15492299]
62. Wuyts FL, Vanhuyse VJ, Langewouters GJ, Decraemer WF, Raman ER, Buyle S. Elastic properties of human aortas in relation to age and atherosclerosis: a structural model. Phys. Med. Biol. 1995; 40:1577–1597. [PubMed: 8532741]
63. Zeller PJ, Skalak TC. Contribution of individual structural components in determining the zero-stress state in small arteries. J. Vasc. Res. 1998; 35:8–17. [PubMed: 9482691]
64. Zuckerman BD, Orton EC, Stenmark KR, Trapp JA, Murphy JR, Coffeen PR, Reeves JT. Alteration of the pulsatile load in the high-altitude calf model of pulmonary hypertension. J. Appl. Physiol. 1991; 70:859–868. [PubMed: 2022578]
65. Zulliger MA, Fridez P, Hayashi K, Stergiopulos N. A strain energy function for arteries accounting for wall composition and structure. J. Biomech. 2004; 37:989–1000. [PubMed: 15165869]

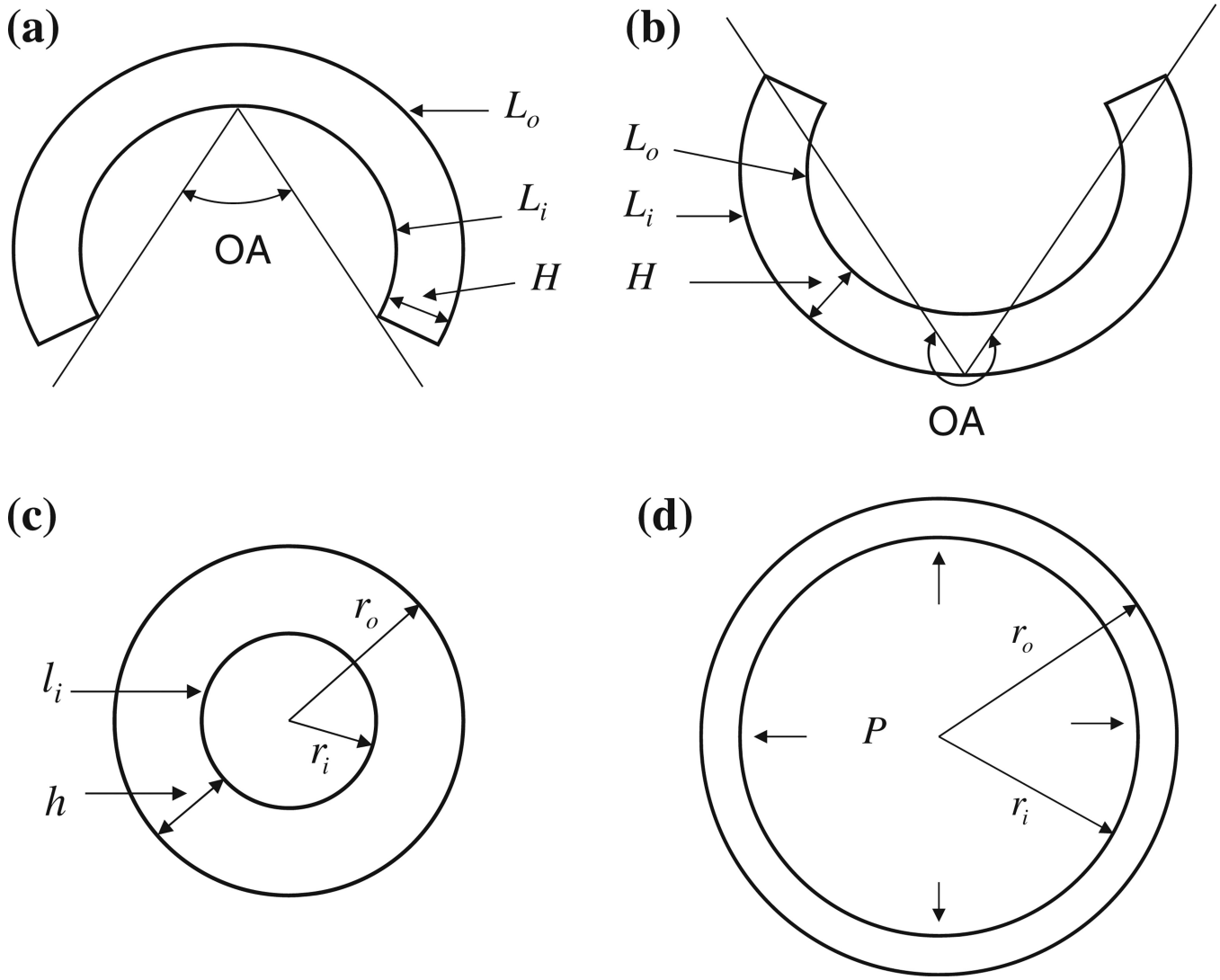

FIGURE 1.
The cross-sectional representations of arteries (a) at the stress-free state with OA<180°, (b) at the stress-free state with OA>180°, (c) at the no-load state and (d) under physiological conditions: *P*, blood pressure.

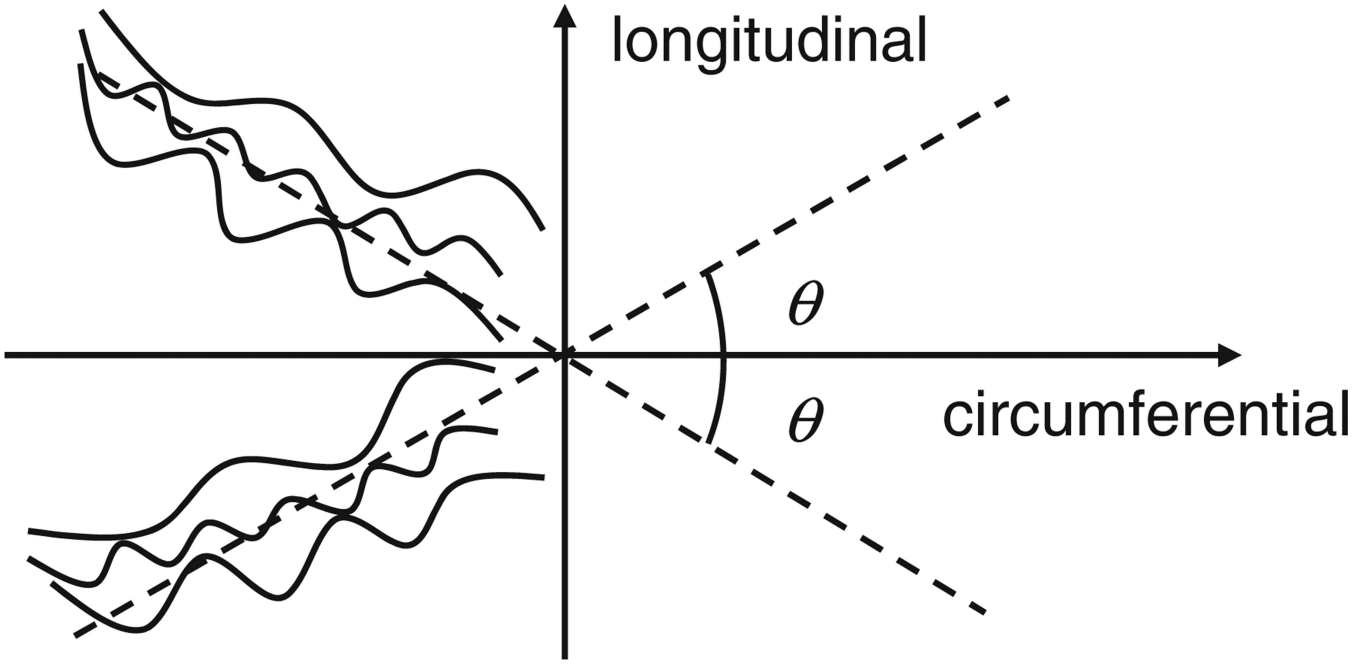

FIGURE 2.
Schematic of the direction of two-family collagen fibers at stress-free state.

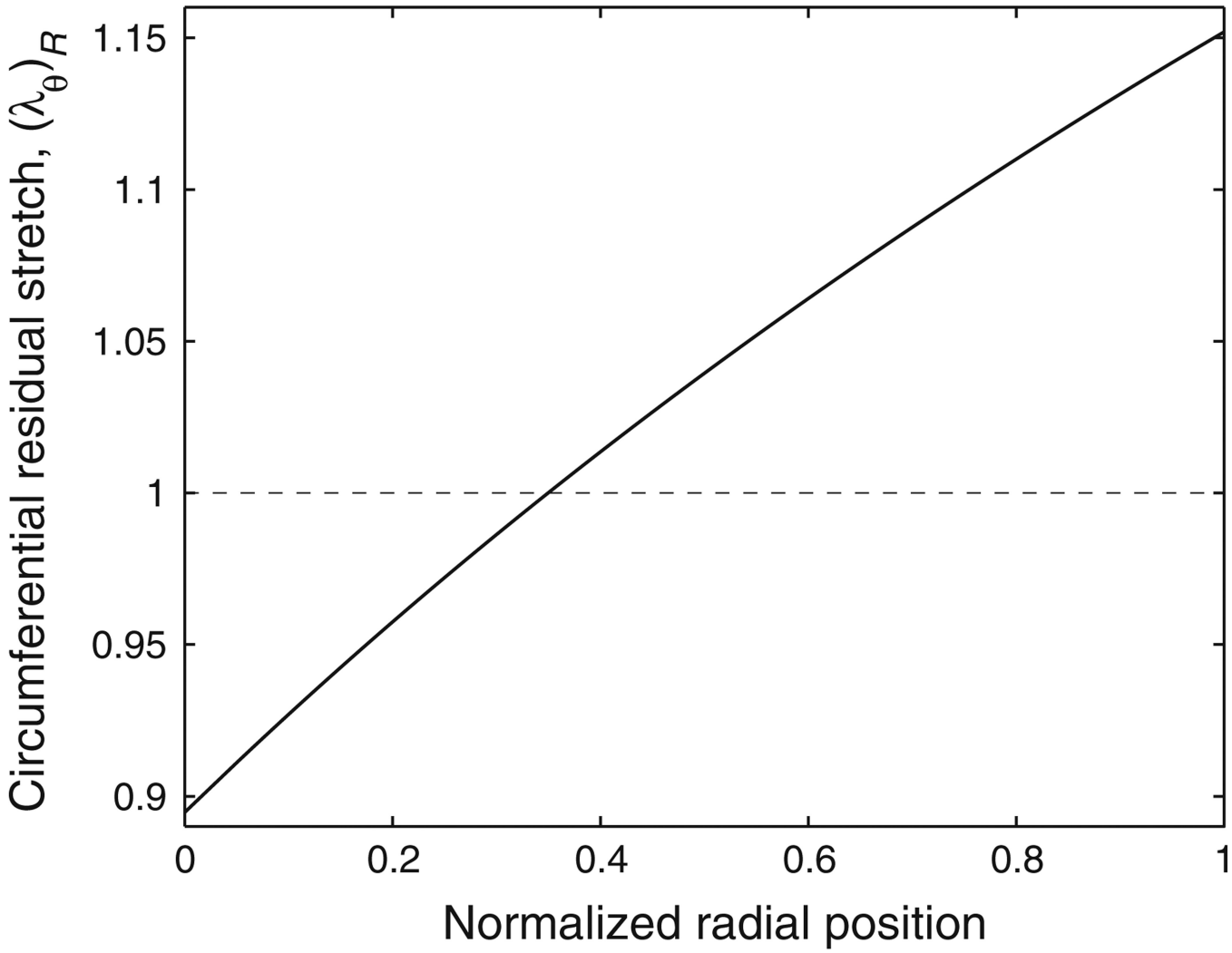

FIGURE 3.
Representative circumferential residual stretch distribution across the vessel wall. Note that the normalized radial position goes from the inner wall (0.0) to the outer wall (1.0).

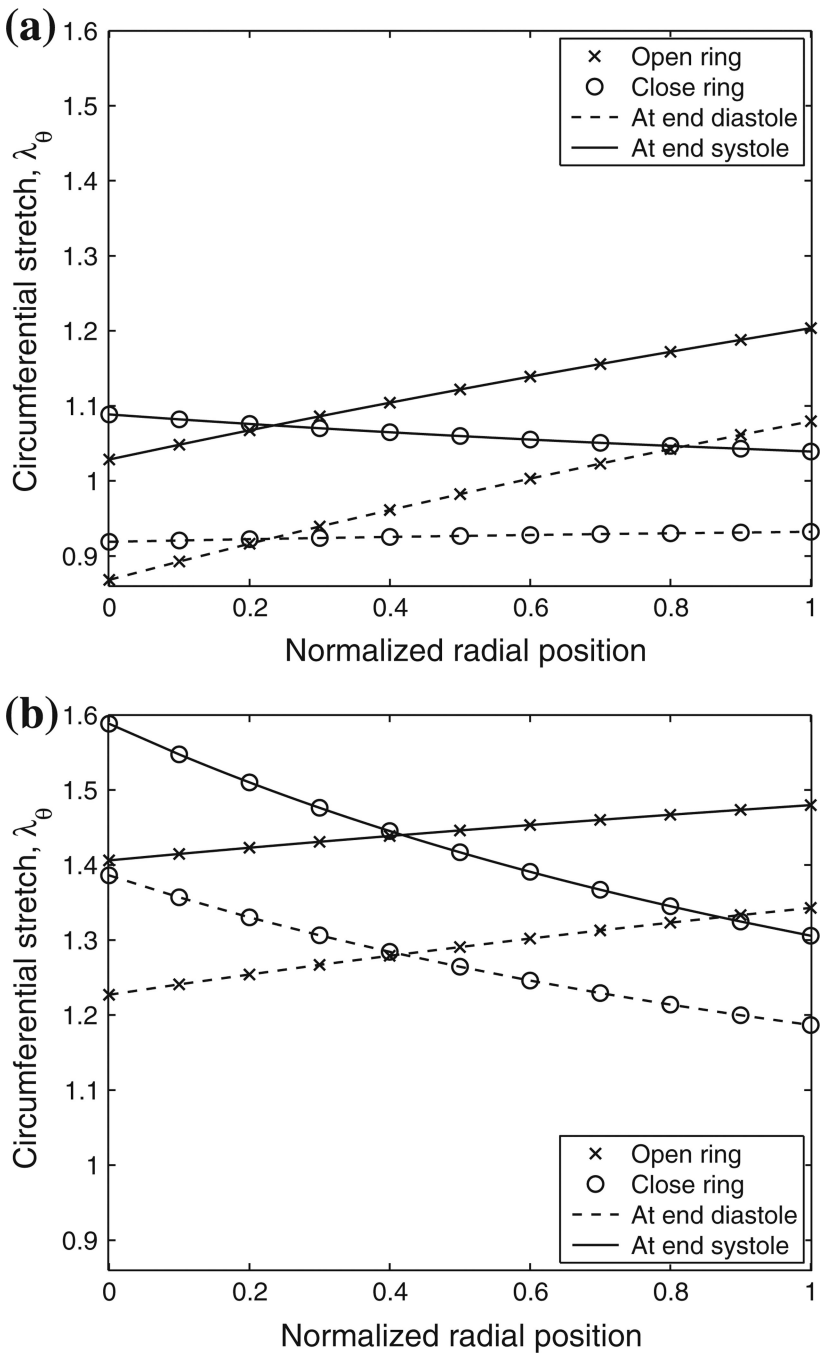

FIGURE 4.

Representative circumferential stretch distributions of calf MPA at end-diastolic and end-systolic pressures and $\lambda_z = 1.1$ with and without residual circumferential stretch (open and close rings in the figures, respectively) considered for (a) control and (b) hypertensive calves. Note that the normalized radial position goes from the inner wall (0.0) to the outer wall (1.0). Also note that a less uniform stretch distribution is observed with residual stretch incorporated in the control calf (Fig. 4a).

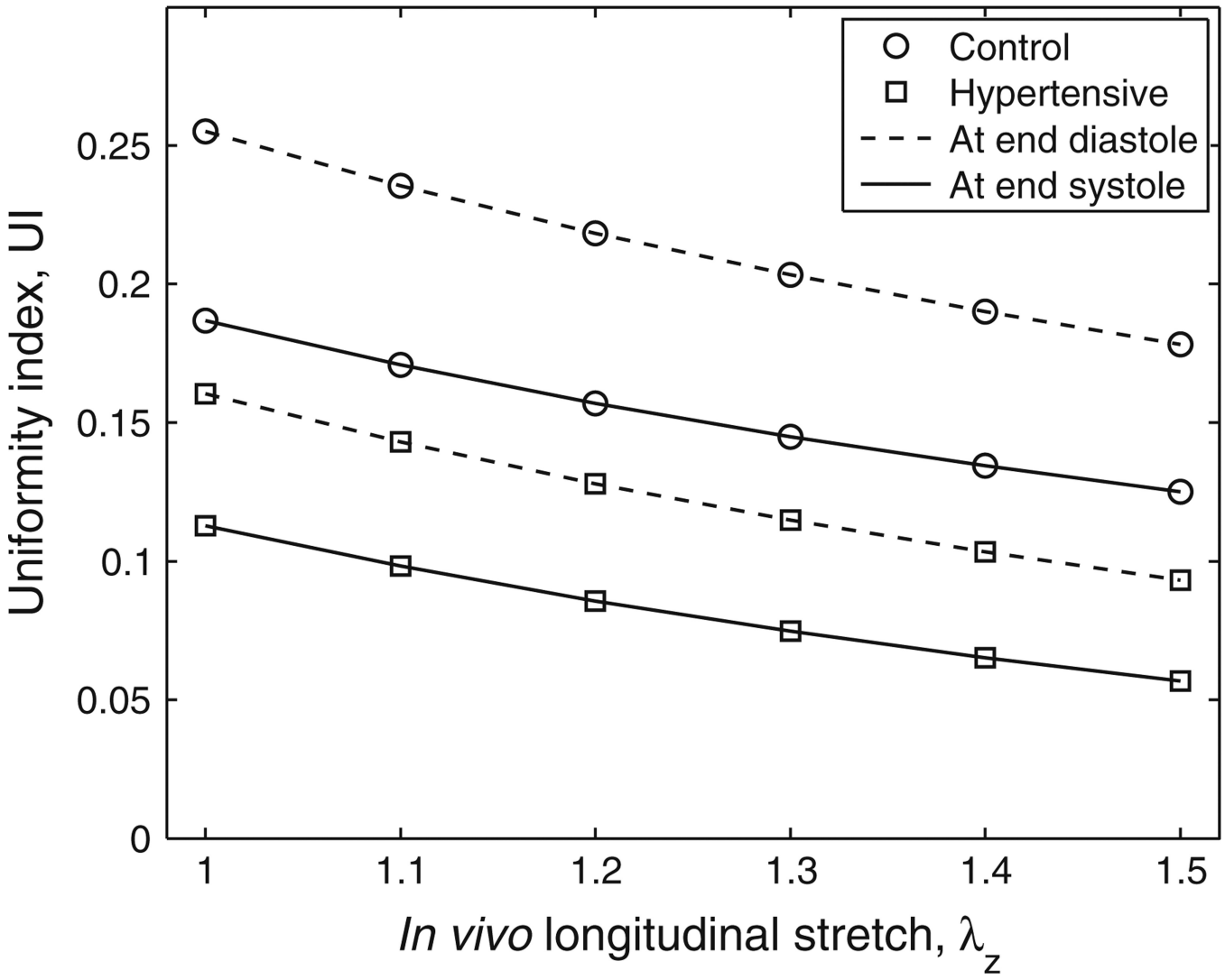

FIGURE 5.
Uniformity index at end diastole and end systole for both groups at different *in vivo* longitudinal stretches. Standard deviations are provided in the text.

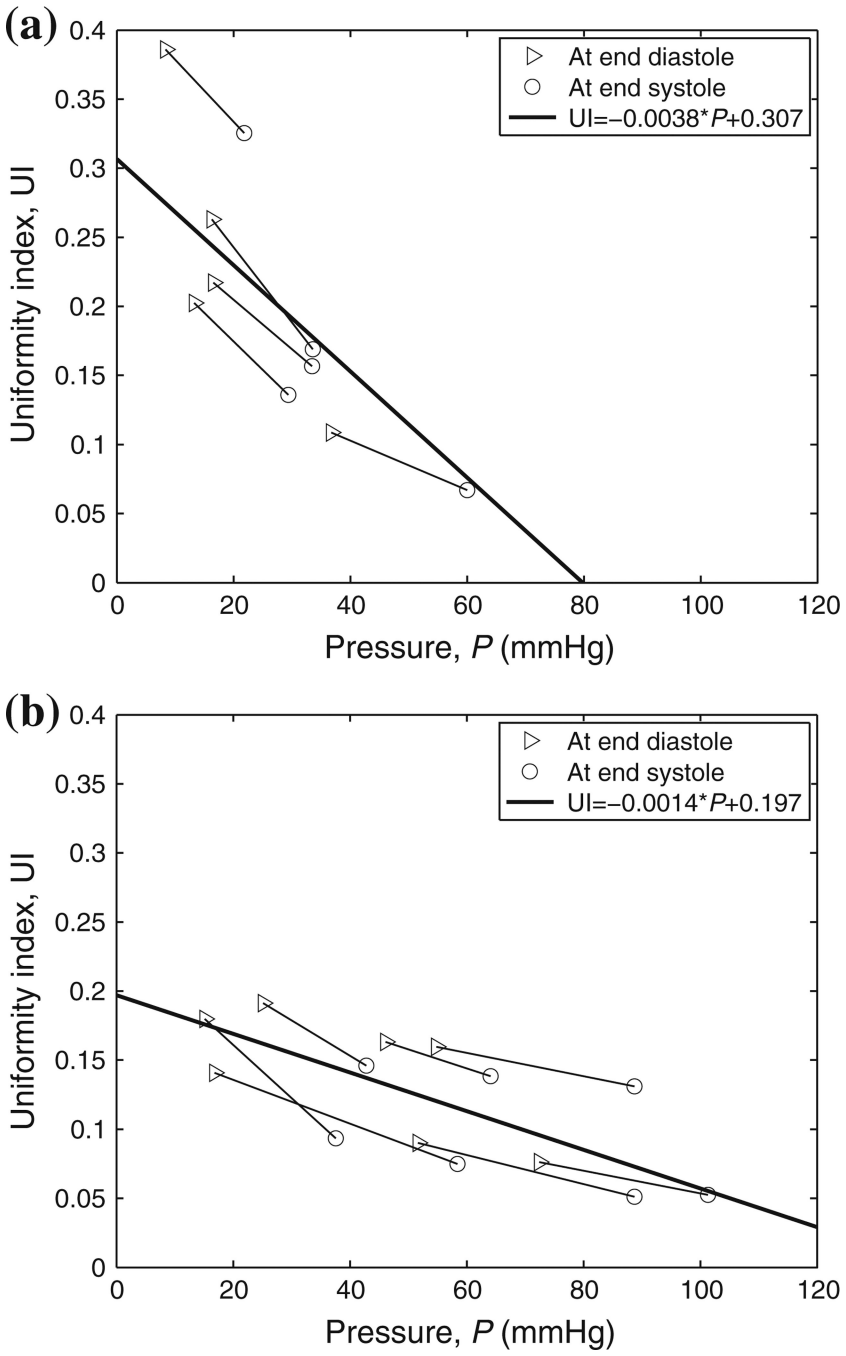

FIGURE 6.

Mixed-effect regression analyses between UI and MPA blood pressure (*P*) for (a) control and (b) hypertensive groups at $\lambda_z = 1.1$. Note that UI = 0 indicates uniform stretch distribution across the vessel wall.

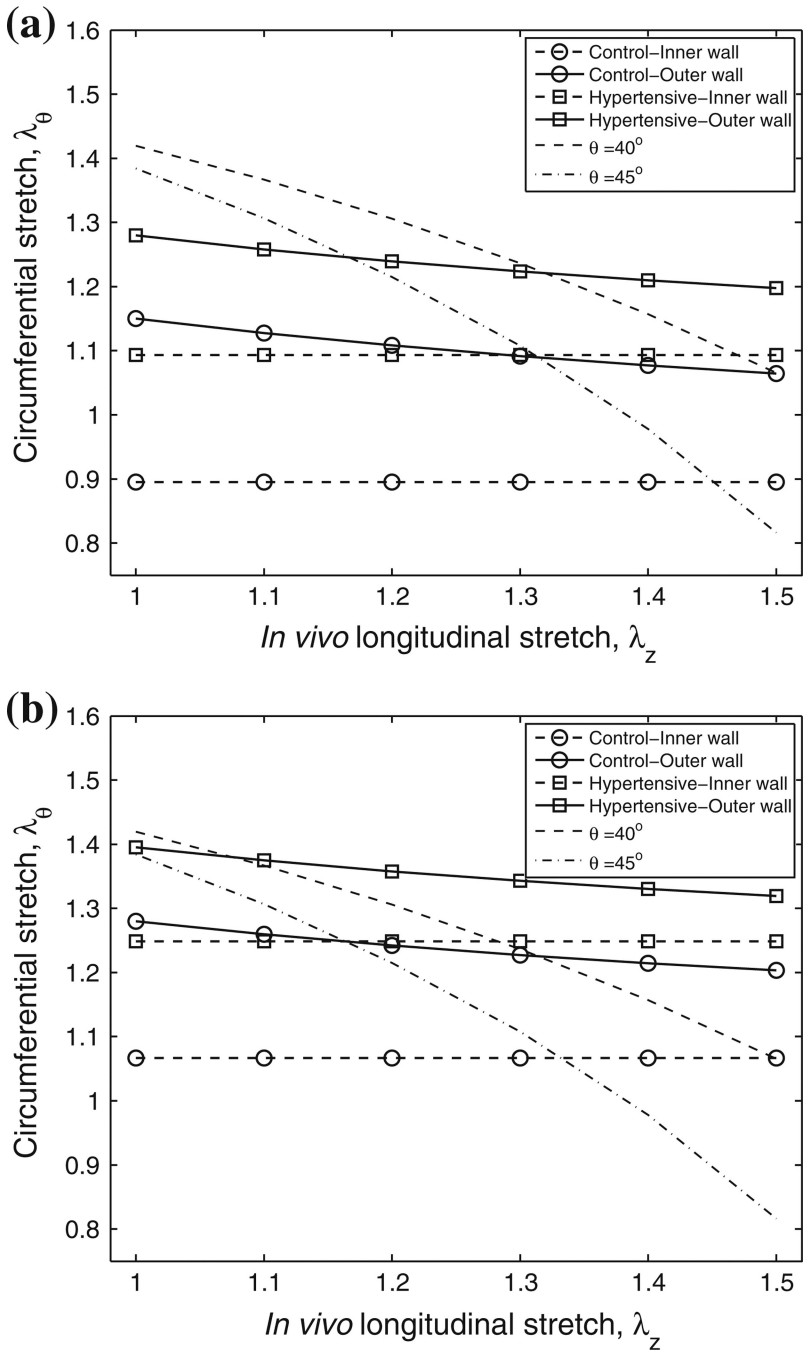

FIGURE 7.

Mean physiological circumferential stretches at the inner and outer walls of the artery at different longitudinal stretches at (a) end-diastolic and (b) end-systolic pressures for control and hypertensive groups and the critical engagement stretches ($\lambda_\theta^{\mathrm{T}}$) with collagen fiber angles at 40° and 45°. Standard deviations are provided in the text.

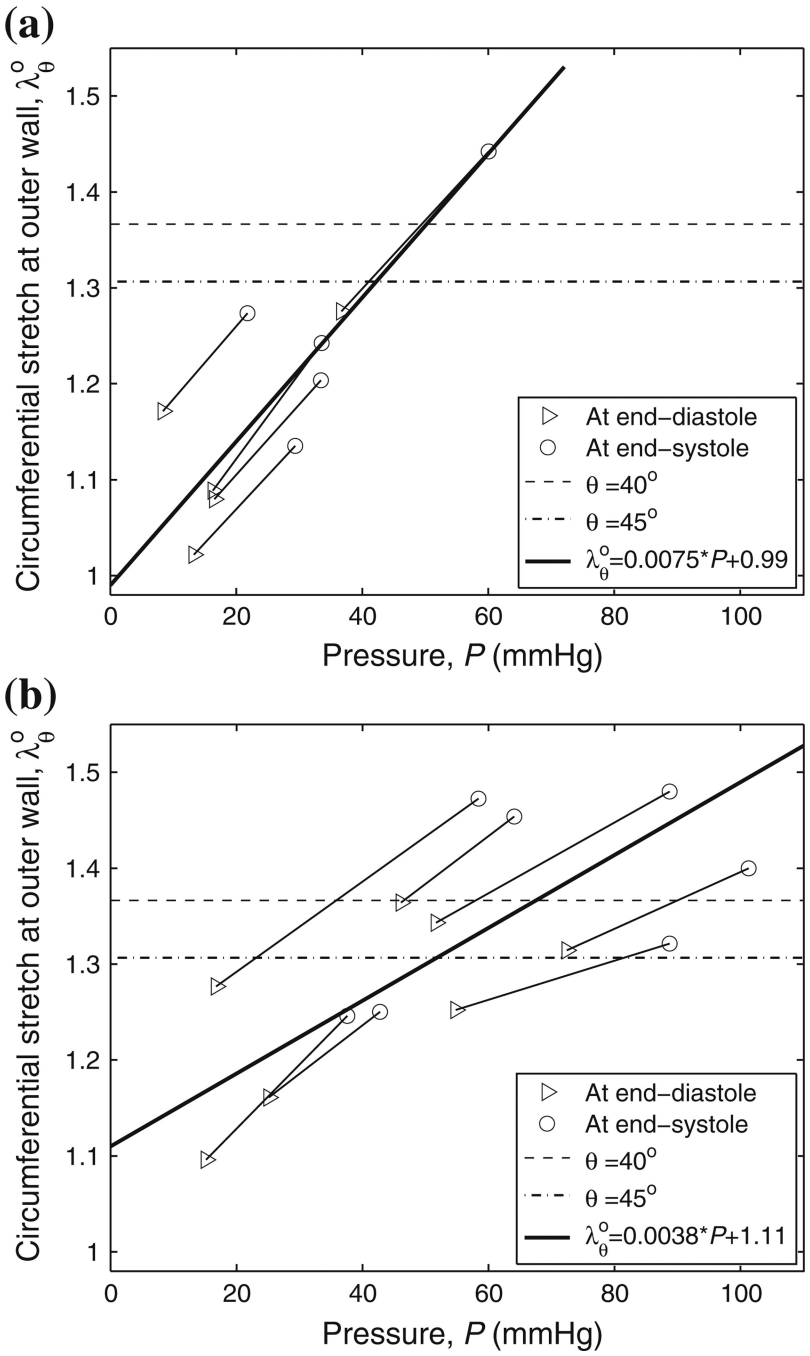

FIGURE 8.

Mixed-effect regression analyses between *in vivo* circumferential stretch at outer wall and MPA blood pressure (*P*) for (a) control and (b) hypertensive groups at $\lambda_z = 1.1$. The dashed and dash-dotted lines are the critical engagement stretches ($\lambda_\theta^{\mathrm{T}}$) with collagen fiber angles at 40° and 45°, respectively.

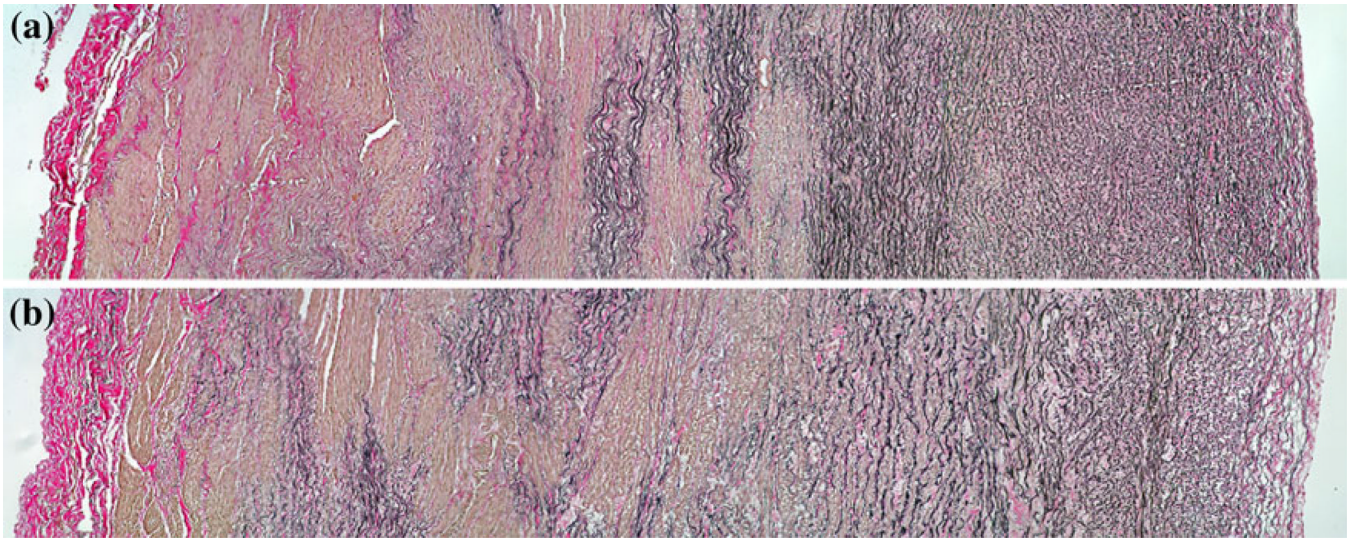

FIGURE 9.
Representative optical microscopy images for (a) control and (b) hypertensive calves. Collagen and elastin appear red and black, respectively. Adventitia and intima are at the left and right sides of the images, respectively.

TABLE 1

Comparison of morphology and residual stretch in MPA between control and hypertensive groups.

	Control (n = 13)	Hypertensive (n = 11)	P value	Equivalent?
mPAP (mmHg)	23.6 ± 9.3	59.9 ± 22.2	**<0.001**	No
ID (mm)	19.4 ± 2.1	19.9 ± 1.4	0.505	**Yes**
h (mm)	3.4 ± 0.3	4.0 ± 0.4	**<0.001**	No
h/ID	0.18 ± 0.03	0.20 ± 0.02	**0.035**	No
OA (degree)	127 ± 38	130 ± 23	0.957	No
$\left(\lambda_\theta^{\mathrm{i}}\right)_{\mathrm{R}}$	0.91 ± 0.06	0.90 ± 0.02	0.820	**Yes**
$\left(\lambda_\theta^{\mathrm{o}}\right)_{\mathrm{R}}$	1.13 ± 0.06	1.15 ± 0.05	0.315	**Yes**

Values are mean ± SD; n, number of arteries; mPAP, mean pulmonary arterial pressure measured at the ambient pressure condition for both groups (n = 8 and 9 for control and hypertensive groups, respectively); ID and h, inner diameter and arterial wall thickness of MPA at no-load state, respectively; OA, opening angle; $\left(\lambda_\theta^{\mathrm{i}}\right)_{\mathrm{R}}$ and $\left(\lambda_\theta^{\mathrm{o}}\right)_{\mathrm{R}}$, residual stretches as calculated by Eq. (4) at the inner and outer walls, respectively. Statistically significant quantities are shown in boldface.